Searches for Cosmic-Ray Electron Anisotropies with the *Fermi*-Large Area Telescope

Vlasios Vasileiou
NASA Goddard Space Flight Center & University of Maryland, Baltimore County

and

Nicola Mazziotta
INFN Bari

on behalf of the *Fermi*-LAT collaboration

The Large Area Telescope (*Fermi*-LAT)

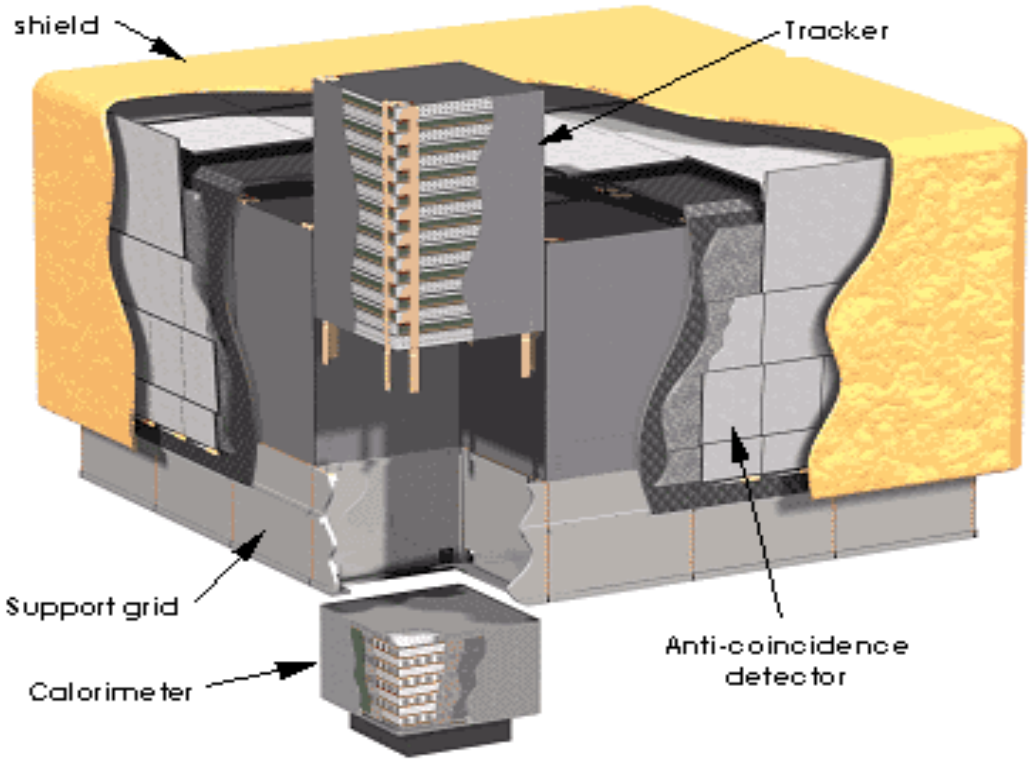

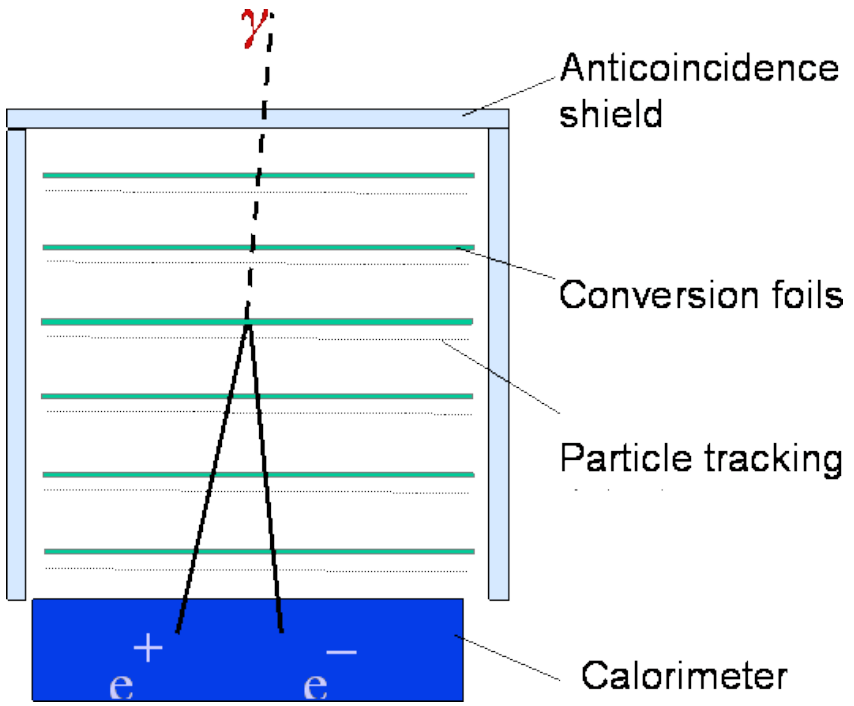

- Pair-conversion gamma-ray detector
  - Tracker + Calorimeter + Anticoincidence Shield
- Primary conceived as a MeV/GeV gamma-ray detector but it can also be a detector for Cosmic Ray Electrons and Positrons (CREs)
- Wide field of view (~2.4sr) + Full-sky coverage (every ~3hrs)

Motivation

- The galactic magnetic field isotropizes the direction distribution of GeV-TeV CRs → information on the direction of CR sources is lost.
- Compared to hadronic Cosmic-Rays, CREs lose their energy rapidly.
  - 100 GeV (1TeV) CREs detected at the earth have originated ***from relatively nearby locations*** at most ~1.6 (0.75) kpc away.
  - Likely to have ***originated from an anisotropic collection of few nearby sources***.
  - Depending on the propagation through the GMF, some anisotropy in the directions of GeV-TeV CREs might still exist.
- Remember: Studies tried to quantify the effect of nearby older pulsars to the detected CRE spectra and to the CR-Positron fraction (e.g. Geminga, Monogem).
  - They predict anisotropies towards the directions of dominant sites of CRE production.
  - ***The discovery of an anisotropy in agreement with the predictions of these studies would be a big step towards revealing the sources of CREs.***

CREs & Magnetic Fields

- The directions of CREs are affected by propagation through the magnetic fields of the galaxy, of the heliosphere, and of the earth.
  - The higher the CRE energy → the smaller the effect.
- **Geomagnetic field**:
  - CREs with energies over the geomagnetic cutoff suffer negligible deflections → ***We used a E>60GeV cut***.
- **Heliospheric Magnetic field**:
  - E<100GeV → appreciable/strong effects
  - E>1TeV → negligible effects
    - We are in between these two extremes.
    - HMF effects not well known → not obvious what minimum energy threshold to use → decide to go ahead with an E>60GeV dataset with the caveat that its low-energy part might have been considerably affected by the HMF (isotropized).

The Dataset

- First year of normal Science Operation (starting August 2008)
- ~1.3 million E>60GeV CRE events
- ~0.1^{o} angular-reconstruction accuracy
- 10% energy resolution
- Low contamination with other species
  - Gammas → <0.1%
  - Hadronic CRs → ~13% (projected anisotropy under our sensitivity)
- All-sky uniform-exposure dataset → allows us to search for anisotropies of ***any angular size (up to dipole) and from any direction in the sky***.

The Anisotropy Search

- We search for anisotropies with no a priori assumptions on the energy, direction, and angular size of the anisotropy.
  - Analyzed multiple subsets of the data: E>60GeV, E>120GeV, E>240GeV, E>480GeV.
  - Started with an all-sky search but also evaluated the sky towards candidate sources (different trials → different sensitivity).
  - Searched for small (~10^{o}) to large scale (90^{o}) anisotropies.

The Anisotropy Search

- Search started with the construction of the ***"no-anisotropy" skymap***:
  - the skymap expected to be detected on-average in the case of a perfectly isotropic CRE distribution → acts as our null hypothesis
- By comparing the no-anisotropy skymap to the actual skymap we could search for anisotropies in the actual data. Two methods were used:
  - Direct bin-to-bin comparison between the two maps.
  - Spherical Harmonic Analysis.
- As as cross-check, two techniques yielding consistent results were used to construct the "no-anisotropy" skymap:
  - Event-Shuffling & Direct-Integration Techniques.
  - Both techniques were based solely on the data (no MC simulations).

Event-Shuffling Technique

- Starts from the original data set and randomly shuffles the reconstructed directions of events (in the instrument frame).
  - The reconstructed energy and direction distributions (in the instrument frame) remain the same.
  - However, ***any anisotropy in sky coordinates is smeared out.***
- The randomization process is repeated multiple times (25), with each iteration producing a skymap that is statistically consistent with the case of an isotropic CRE direction distribution.
- These skymaps are then averaged, to construct the final no-anisotropy skymap.
- The technique is simple to implement and straight forward. It also has the benefit of automatically taking care of any short-term variations of the detector's effective area.

Direct-Integration Technique

- In general, the rate of events from some direction in instrument coordinates (θ,φ) is equal to the all-sky rate $R_{allsky}(t)$ times the probability that an event is reconstructed at that direction $P(\theta,\varphi,t)$.
- Based on the above, given a value for these two variables and the pointing information of the instrument, we can construct an associated skymap.
- What we want to do is to find the value of these variables that corresponds to the case of a perfectly isotropic CRE direction distribution, and using this value construct the no-anisotropy skymap. Which is this value?
  - ✗ As an anisotropy passes through the LAT's FOV, it creates fluctuations in the ***instantaneous value*** of these variables.
  - ✔ However, their ***averaged-over-multiple-orbits value*** remains constant, since any anisotropy events are averaged out.

Method #1: Direct Bin-to-Bin Comparison

- By construction, started with ~1° *independent-bins* skymaps.
  - Can't search for tens-of-degs anisotropies with such skymaps (spillover effects reduce sensitivity).
- Produced several *integrated* skymaps, each with a different integration radius: 10°, 30°, 45°, 60°, 90°.
- Then, a bin-to-bin comparison between the actual and the predicted for the case of no anisotropy skymaps was performed:
  - For each pair of bins in the actual and the no-anisotropy skymap with contents $n_{sig,i}$ and $n_{iso,i}$ respectively, we calculated the probability of detecting a number of events at least as small as $n_{sig,i}$ while expecting $n_{iso,i}$.
  - For the Event-Shuffling technique we used Li & Ma significances. For the Direct-Integration technique we used simple Poisson probabilities.

Effective number of trials

- We calculated the effective number of trials involved in evaluating the 12,288 possible directions (number of bins) in an integrated significance skymap.
- These data were produced by simulating randomized significance skymaps and counting the fraction of such skymaps (P_{post}) that a probability less or equal than (P_{pre}) was found.

$$T_{eff} = \frac{log(1 - P_{post})}{log(1 - P_{prc})}.$$

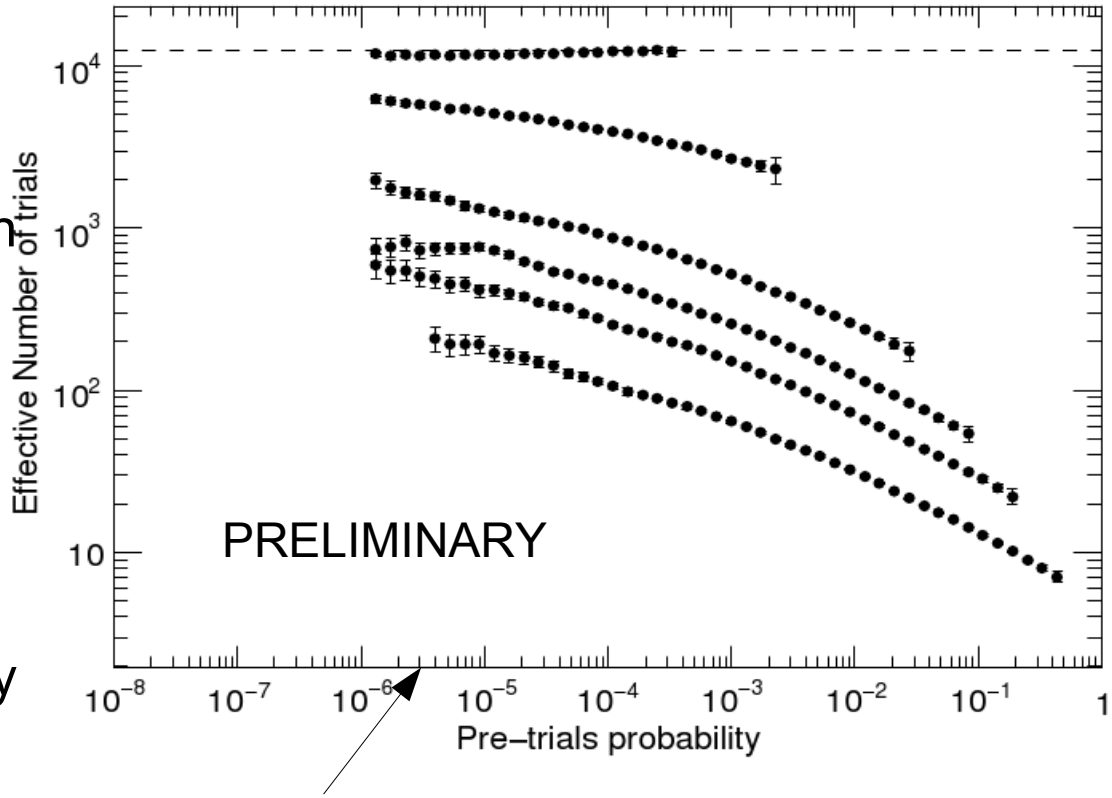

- Each curve shows the effective number of trials for a different integration radius.
- From top to bottom: independent-bins case, 10°, 30°, 45°, 60°, 90° integration radius.

Sensitivity of the Bin-to-Bin Search

- Effective number of trials + number of events in the dataset → sensitivity.
- The sensitivity becomes worse for smaller integration radii because the effective number of trials increases.
- The sensitivity becomes worse for higher energies because of the worse statistics.
- ***Sensitivity for a dipole anisotropy ranges from ~10% to a fraction of a pct.***

PRELIMINARY

- Fractional excess needed for the bin-to-bin comparison method to detect an anisotropy with a 3σ post-trials significance.

A Significance Skymap

- A **pre-trials** significance map produced by a bin to bin comparison of the no-CRE-anisotropy to the actual skymap
- Integration radius 45^{o} & Energy>60GeV
- Because of the large number of trials all the observed fluctuations are ***post-trials insignificant.***

PRELIMINARY

Results of the bin-to-bin comparison

- **Curves:** Correspondence between a pre and a post-trials significance. Left to right 90°, 60°, 40°, 30°, 10° integration radius.
- **Markers:** Best significance in each of the different tests.

PRELIMINARY

All the results were post-trials insignificant.

- An evaluation of the maps towards interesting locations (Geminga, Vela, Monogem pulsars, and the Galactic and anti-galactic centers) also yielded null results. Best post-trials significance ~1.6σ from anti-galactic center.

Method #2: Spherical Harmonic Analysis

- Spherical harmonic analysis of a fluctuation map produced by dividing the signal with the no-anisotropy skymap.
  1. The fluctuation map was first expanded in the basis of spherical harmonics, producing a set of a_{lm} coefficients.
  2. The average variance of these coefficients was used to construct an angular power spectrum.
  3. The power spectrum was compared to the expected spectrum of a white-noise data set (applicable for an isotropic sky).
  4. An increased power at a multipole *l* would indicate the presence of an anisotropy in the data would half-angular scale ~90°//.

Power Spectra

- **Markers**: Power spectra from both techniques for E>60GeV.
- **Curves:** Ranges that show the 3σ and 5σ integrated-probability fluctuations of a white-noise spectrum.
- All the spectra were consistent with being mere statistical fluctuations of an isotropic signal.

PRELIMINARY

Conclusion

- We searched for anisotropies in the reconstructed directions of ~1.3 million CREs detected by the *Fermi*-LAT during its first year of operation.
- Both methods used to perform the search resulted to null results.
- Upper limits on the degree of anisotropy were set (not presented).
- The analysis and results to be published soon.

THANK YOU!

Contamination

TABLE I. Geometry factor, residual contamination, number of counts before background subtraction, and the flux J_E multiplied by E^3. The statistical error is followed by the systematic error. The latter does not include the effect due to the uncertainty in the absolute energy scale (see text).

Energy (GeV)	GF (m^2 sr)	Residual contamination	Counts	$E^3 J_E$ (GeV^2 s^{-1} m^{-2} sr^{-1})
23.6–26.0	1.65	0.04	478 929	$151.6 \pm 1.2^{+7.3}_{-8.3}$
26.0–28.7	2.03	0.05	502 083	$152.6 \pm 0.9^{+6.2}_{-7.3}$
28.7–31.7	2.35	0.05	487 890	$151.4 \pm 0.8^{+5.1}_{-6.5}$
31.7–35.0	2.59	0.09	459 954	$151.3 \pm 1.8^{+5.2}_{-6.5}$
35.0–38.8	2.67	0.07	385 480	$149.6 \pm 0.7^{+4.4}_{-5.8}$
38.8–43.1	2.72	0.08	330 061	$150.2 \pm 0.7^{+4.5}_{-6.0}$
43.1–48.0	2.76	0.10	276 105	$148.6 \pm 0.7^{+4.9}_{-6.2}$
48.0–53.7	2.79	0.11	233 877	$146.5 \pm 0.7^{+4.9}_{-6.1}$
53.7–60.4	2.77	0.12	194 062	$145.5 \pm 0.7^{+5.0}_{-7.1}$
60.4–68.2	2.76	0.13	155 585	$143.2 \pm 0.7^{+5.6}_{-6.8}$
68.2–77.4	2.73	0.14	126 485	$141.9 \pm 0.8^{+5.6}_{-7.0}$
77.4–88.1	2.71	0.14	100 663	$140.8 \pm 0.8^{+6.2}_{-7.0}$
88.1–101	2.68	0.15	77 713	$139.0 \pm 0.9^{+6.4}_{-6.8}$
101–116	2.64	0.16	61 976	$139.0 \pm 0.9^{+6.4}_{-7.2}$
116–133	2.58	0.17	46 865	$139.4 \pm 1.0^{+6.9}_{-7.2}$
133–154	2.52	0.17	35 105	$139.5 \pm 1.2^{+7.2}_{-7.4}$
154–180	2.44	0.17	27 293	$140.8 \pm 1.3^{+6.9}_{-7.4}$
180–210	2.36	0.18	19 722	$142.3 \pm 1.5^{+7.1}_{-7.4}$
210–246	2.27	0.18	13 919	$140.9 \pm 1.7^{+7.4}_{-6.8}$
246–291	2.14	0.18	10 019	$140.9 \pm 1.9^{+7.5}_{-6.7}$
291–346	2.04	0.18	7207	$140.4 \pm 2.2^{+6.7}_{-7.0}$
346–415	1.88	0.18	4843	$139.4 \pm 2.6^{+7.0}_{-7.2}$
415–503	1.73	0.19	3036	$134.0 \pm 3.1^{+9.3}_{-7.5}$
503–615	1.54	0.20	1839	$127.4 \pm 4.1^{+8.7}_{-8.6}$
615–772	1.26	0.21	1039	$115.8 \pm 4.8^{+15.2}_{-10.9}$
772–1000	0.88	0.21	544	$114.4 \pm 6.5^{+19.1}_{-17.8}$

Energy Resolution

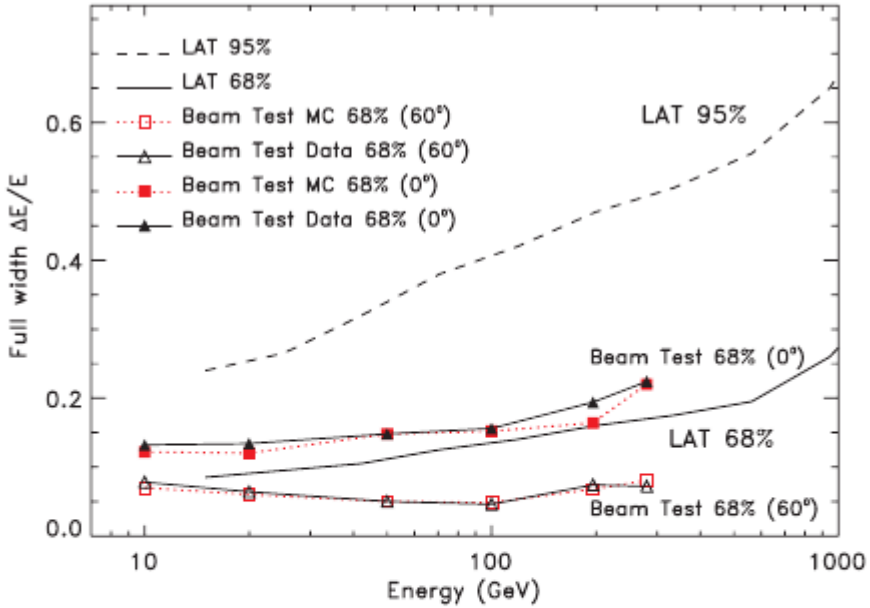

FIG. 1 (color online). Energy resolution for the LAT after electron selection; the full widths of the smallest energy window containing the 68% and the 95% of the energy dispersion distribution are shown. The comparison with beam test data up to 282 GeV and for on-axis and at 60° incidence shown in the figure indicates good agreement with the resolution estimated from the simulation.